Biofabrication

PAPER

Micropocket hydrogel devices for all-in-one formation, assembly, and analysis of aggregate-based tissues

Lisa Zhao[1], Stephanie Mok[1] and Christopher Moraes[1,2,3]

[1] Department of Chemical Engineering, McGill University, Montréal, Canada
[2] Department of Biological and Biomedical Engineering, McGill University, Montréal, Canada
[3] Goodman Cancer Research Center, McGill University, Montréal, Canada

E-mail: chris.moraes@mcgill.ca

RECEIVED
18 March 2019

REVISED
26 June 2019

ACCEPTED FOR PUBLICATION
9 July 2019

PUBLISHED
13 August 2019

Keywords: microfabrication, tissue engineering, 3D printing, replica molding, hydrogel, spheroid, 3D migration

Supplementary material for this article is available online

Abstract

Multicellular aggregated tissues have grown critically important in benchtop biomedical research, both as stand-alone spheroids and when assembled into larger bioengineered constructs. However, typical systems for aggregate formation are limited in their capacity to reliably handle such cultures at various experimental stages in a broadly accessible, consistent, and scalable manner. In this work, we develop a broadly versatile all-in-one biofabrication strategy to form uniform, spherical, multicellular aggregates that can be maintained at precisely defined positions for analysis or transfer into a larger tissue. The 3D-printed MicroPocket Culture (MPoC) system consists of an array of simple geometry-based valves in a polyacrylamide hydrogel, and is able to produce hundreds of uniformly-sized aggregates in standard tissue culture well plates, using simple tools that are readily available in all standard biological wet-labs. The model breast cancer aggregates formed in these experiments are retained in defined positions on chip during all liquid handling steps required to stimulate, label, and image the experiment, enabling high-throughput studies on this culture model. Furthermore, MPoCs enable robust formation of aggregates in cell types that do not conventionally form such structures. Finally, we demonstrate that this single platform can also be used to generate complex 3D tissues from the precisely-positioned aggregate building blocks. To highlight the unique and broad versatility of this technique, we develop a simple 3D invasion assay and show that cancer cells preferentially migrate towards nearby model tumors; demonstrating the importance of spatial precision when engineering 3D tissues. Together, this platform presents a broadly accessible and uniquely capable system with which to develop advanced aggregate-based models for tissue engineering, fundamental research, and applied drug discovery.

Introduction

The use of three-dimensional (3D) tissue engineering and culture techniques is rapidly gaining recognition as being critically important to study cells in realistic culture environments. Multicellular aggregates of cells have emerged as a relatively accessible culture model for certain 3D tissues such as cancer tumors [1–6], stem cell differentiation models [7–9], and drug screening [3, 4, 10–13], as they can recapitulate various tumor features including internal gradients of signaling factors, nutrients, and oxygenation. Furthermore, they can also serve as building blocks to create more complex tissues for implantation [14] or fundamental studies of cell behavior [15].

Widespread use of multicellular aggregate cultures is limited because these cultures are intrinsically harder to handle than standard 2D culture plates. Multicellular aggregates are typically formed on a per-aggregation basis using pipetting-based techniques, such as the hanging drop method [11, 16] or aqueous two-phase based compartmentalization [17–20], in which adherent cells cannot bind to external surfaces and are hence forced to aggregate together. These techniques are readily adoptable but present difficulties in scaling up, as the arrayed techniques require a

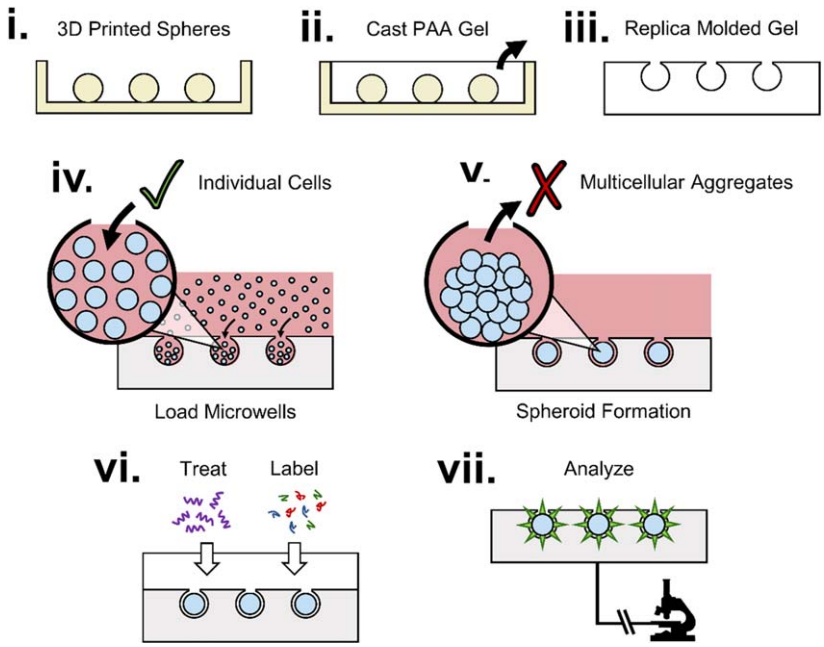

Figure 1. Micro Pocket Culture (MPoC) technique overview. To fabricate the described devices, (i) a negative mold is fabricated using a digital light projection stereolithography 3D printer. (ii) A polyacrylamide (PAAm) gel is cast, polymerized, and (iii) removed from the mold, retaining partial spherical pockets in the device. (iv) Cells are seeded in suspension and are sufficiently small to enter and settle into the pockets. (v) Once cells aggregate together, they are too large to leave the pocket, and are retained in their pre-defined positions during regular handling and culture manipulation. (vi) Aggregates can then be treated, labeled, or embedded in extracellular matrix directly on the MPoC chip; and (vii) analyzed by optical techniques.

pipetting operation to form each aggregate and additional pipette operations per aggregate for routine experimental steps like washing, labeling, treating, and imaging the cultures. Scaled-up methods have been introduced, including forming aggregates in non-adhesive microwells [21] or in stirred vessels [1, 21–23], but these stochastic techniques have relatively poor control over aggregate size, which is a critically important parameter for aggregate function. More technically advanced strategies such as the use of microarrayed [3, 7, 24–26] or microfluidic systems [27–31] have also been developed to provide controlled and addressable culture models, but these are challenging to adopt in standard wet labs as microfluidic systems typically require considerable expertize to fabricate and operate [32].

The core challenge to address in each of these multicellular aggregate culture systems is that of handling the aggregates during formation, culture, and analysis; in a manner that is simple, robust, consistent, and scalable (reviewed in [33]). In most readily accessible platforms, the aggregates are free to move during liquid handling; which makes standard operations like washing, labeling, stimulating, and imaging the aggregates prone to accidental sample loss and damage [34]. This can be particularly challenging for experiments involving rare or precious samples. In more advanced microengineered platforms, aggregates are maintained in 'trap' structures (reviewed in [35]) that necessitate careful control over fluid flow, and hence requires technical expertize to build and operate.

To address these issues, and inspired by recent work in which a nylon mesh was used to hold spheroids within microwells [36], we designed an extremely simple, passive one-way hydrogel 'valve' that allows individual cells to enter a microfabricated spherical chamber, but prevents them from leaving once aggregated (figure 1). The open-faced design of this 'Micro Pocket Culture' (MPoC) system works with standard pipette-based handling techniques available in most wet labs, and allows aggregates to be maintained in precisely defined positions, even during vigorous washing and liquid handling steps. Hence, aggregates can be handled across the entire life-cycle of the experiment, including formation, treatment, labeling, and analysis. Uniquely, the hydrogel-based pocket design allows the precisely-positioned aggregates to be transferred into an embedding extracellular matrix directly on the device, enabling integrated and precise production of tissues using aggregates as building blocks.

To realize this proposed device, we leveraged the functionality of a readily-accessible 3D printer to microfabricate a template mold with overhanging structures. We then replica molded these spherical features in polyacrylamide, a well-established hydrogel for long-term culture that does not allow cell attachment and permits nutrient and oxygen transport [37, 38] into the micropocket chamber. To demonstrate the utility of this system, we characterized aggregate formation for three commonly used breast cancer cell lines in the devices, demonstrated

immunostaining and aggregate stimulation with a candidate chemotherapeutic agent, and compared them to aggregates formed using alternative strategies. Finally, we demonstrate the utility of this all-in-one system for precision-3D tissue engineering.

Methods

Unless otherwise stated, all cell culture materials and supplies were purchased from Fisher Scientific (Ottawa, ON), and chemicals from Sigma Aldrich (Oakville, ON).

3D printed master molds

Arrayed micropocket master molds were designed in AutoCAD and 3D printed with an AutoDesk Ember STL 3D printer. PR-57K black resin (Colorado Photopolymer Solutions) was used and parts were sliced at a layer thickness of 10 μm, with a modified model layer exposure time of 0.76 s. The completed parts were rinsed with isopropyl alcohol and cured under a 36 W UV light for 24 h.

Preparation of MPoC platforms

To provide a substrate with which to handle and bond to the polyacrylamide (PAAm) gels, 18 mm glass coverslips were silanized by submersion in a solution of 0.4% 3-(trimethoxysilyl)propyl methacrylate in acetone for 5 min, followed by a 5 min rinse in acetone. This step modifies the glass surface to covalently bind polyacrylamide hydrogels during polymerization [39]. The coverslips were then removed, air-dried, and stored until use. 3D printed molds were rinsed with reverse osmosis-purified water and dried with an air gun prior to PAAm replica molding. PAAm gels were formed using established protocols [40]. Briefly, a PAAm prepolymer solution of 300 μl 40% Acrylamide stock solution (Bio-Rad), 120 μl of 2% Bisacrylamide stock solution (Bio-Rad), 478 μl of phosphate buffered saline (PBS), and 1.5 μl of Tetramethylethylenediamine were mixed in a 1.5 ml Eppendorf tube. Immediately prior to molding, 100 μl of freshly-prepared 1% w/v ammonium persulfate initiator was added to the solution. The unpolymerized solution was pipetted to completely fill the 3D printed molds and silanized cover slips were placed on top of the molds. After waiting 8 min for the PAAm to gel, the coverslips were peeled away with MPoC devices attached. Devices were rinsed in PBS three times for 5 min each, and stored for at least 24 h in excess PBS to eliminate any residual acrylamide, which may cause undesired toxic effects [41, 42]. The resulting devices were stored in 12-well plates in PBS at room temperature until use. All devices were sterilized while still in PBS in a UV chamber at 36 W for 30–45 min prior to cell culture.

Cell culture

Three breast cancer cell lines, MDA-MB-231, MCF-7, and T-47D (ATCC) were used in the described experiments. Cells were cultured in T-25 vented cap cell culture flasks (VWR). All cells were maintained in Dulbecco's Modified Eagle's Medium (DMEM) high glucose supplemented with 10% (v/v) fetal bovine serum and 1% (v/v) antibiotic-antimycotic (37 °C, 5% CO_2). Culture media was changed every two days. When cells reached approximately 80% confluency, trypsin-EDTA (0.25%) was used to dissociate cells. Cells were resuspended in complete growth medium to the desired cell concentration.

MPoC seeding and aggregate formation

MDA-MB-231, MCF-7, and T-47D cells were each prepared in a 5×10^6 cells ml^{-1} suspension in complete media for all standard seeding experiments. Excess PBS hydrating the MPoC chips was aspirated and devices were transferred to a fresh 12-well plate. 80 μl droplets of each cell suspension was pipetted onto the surface of each device. The droplets were left for approximately 5 min to allow cells to settle by gravity into the microwells. Next, PBS was used to gently wash away excess cells on the surface of the devices and 1 ml of complete media was added to each well. The well plate was incubated at 37 °C and 5% CO_2 for at least 24 h to allow for cells to form aggregates and spheroids.

Hanging drop and aqueous two-phase aggregate formation

For both hanging drop and aqueous two-phase system (ATPS) aggregate formation [19], tissue culture surfaces were made hydrophobic to prevent cell adhesion. A 0.2% (w/v) solution of Pluronics F108 (BASF) in PBS was pipetted onto Petri dish lids and onto round-bottomed 96 well plates and left to sit for 1 h at room temperature. Plasticware was then rinsed with water before letting it air dry. In hanging drop aggregation methods, cells were placed in a droplet of media with no non-cellular surfaces present on which to form attachments. To achieve this, 10 μl droplets of cell suspension (1×10^6 cells ml^{-1}) were carefully pipetted on the inside lid of a 60 mm polystyrene petri dish. The bottom of the dish was filled with PBS to provide a humidified environment before carefully flipping the lid and replacing it on the dish. Cell aggregates were left to form in an incubator for 48 h. In the ATPS method, cells are kept highly localized within an immiscible fluid droplet, encouraging them to aggregate. To implement this technique, we followed existing protocols [19]. Briefly, a polyethylene glycol (PEG) and dextran (DEX) aqueous pairing was used with cells in the dextran phase. PEG stock solutions were prepared by mixing 6% (w/v) PEG in complete media, and diluted 9:1 in media to prepare the final PEG phase solution. 15% (w/v) DEX stock solutions

were prepared in PBS. 50 μl of PEG stock was dispensed into each round-bottom well. 85 μl of a 17 $\times$ 10^6 cells ml^{-1} suspension was mixed with 15 μl of the DEX solution in a separate Eppendorf tube. 1 μl drops of the cell-dextran mixture were dispensed into each well. The plate was then left to settle in the incubator for 1 h. 75 μl of complete media was then added to each well. The spheroids were incubated for 48 h before analysis.

Tissue sectioning and staining

Aggregates were fixed in 4% w/v paraformaldehyde and stored in PBS at 4 °C. Fixed aggregates were embedded in paraffin wax, sliced into 4 μm thick sections, and mounted on clean glass microscope slides. Haemotoxylin and eosin (H&E) staining was conducted following standard protocols.

Fluorescent labeling

Aggregates were labeled for E-cadherin, F-actin, and nuclei after 24 h in culture, using standard indirect immunostaining techniques. MPoC chips were washed twice in PBS and fixed in 4% (v/v) paraformaldehyde in PBS for 1 h at room temperature. Chips were washed twice with PBS for 5 min each and permeabilized with 0.1% (v/v) Triton-X in PBS for 1 h at room temperature. After washing 2 times with PBS for 5 min each again, the spheroids were blocked against non-specific binding with 2.5% (v/v) goat serum in PBS for 1 h at room temperature. Devices were then incubated overnight at 4 °C with anti-E-cadherin monoclonal antibodies (ab1416; Abcam) in a 1:200 dilution of goat serum. To minimize amounts of primary antibody required, MPoC devices were placed upright on top of parafilm and 200 μl of the antibody solution was dispensed on top of the device. The parafilm allowed the droplet to remain a bubble over the entire device. After incubation, MPoC devices were transferred back into a well plate and washed twice with PBS for 10 min each and blocked with 2.5% (v/v) goat serum in PBS for 1 h. After blocking, samples were incubated at room temperature for 2 h with goat anti-mouse IgG secondary antibodies (ab150116; Abcam) in a 1:1000 goat serum dilution. Samples were rinsed for 10 min in PB and counterstained with Hoechst 33258 nuclear DAPI stain (2 μg ml^{-1} in PBS) and phalloidin-FITC (0.005 μl ml^{-1} in PBS) for 1 h at room temperature. Devices were washed twice with PBS and imaged in an Olympus IX73 spinning disc confocal microscope.

Paclitaxel treatment and analysis

To demonstrate that drug treatment can be conducted *in situ*, we treated aggregates in MPoCs with a candidate chemotherapeutic: paclitaxel. After 2 days of aggregate culture in complete media, culture media was replaced with either DMSO in complete media as a vehicular control (1:1000) or 100 μM paclitaxel in complete media. Aggregates were treated with paclitaxel for 24 h. Aggregates still in MPoC chips, were live/dead stained with calcein AM (2 μM in PBS) and ethidium homodimer-1 (EthD-1; 4 μM in PBS) for 1 h at room temperature. Devices were washed once with PBS and imaged. The number of dead cells with and without paclitaxel were manually quantified from the resulting confocal images.

MPoC-based engineered tissues and invasion assays

MPoC chips containing aggregates formed over 24 h were overlaid with collagen gels to produce 3D tissues containing aggregates positioned in defined locations. Media was aspirated from each device and collagen was polymerized using established protocols [43]. Briefly, Type I bovine collagen (Advanced Biomatrix, 3 mg ml^{-1}) was diluted to 2 mg ml^{-1} in PBS and 10$\times$ DMEM solution to obtain a final 1$\times$ DMEM concentration and kept on ice. The acidic solution was neutralized with 3 M NaOH by titration based on the color of the phenolphthalein indicator in DMEM. Cold collagen gel solution was pipetted over the MPoC devices and allowed to incubate at 37 °C for 45 min to gel. After gelation, 1 ml of complete media, with or without 5 ng ml^{-1} of transforming growth factor (TGF)-β1 or 50 ng ml^{-1} of Hepatocyte Growth Factor (HGF; PeproTech; Montreal, QC, Canada) was added to each well to stimulate invasion. Tissues were incubated for 24 h, fixed, stained for nuclei and phalloidin, and imaged as previously described. Cell density was quantified by nuclear count and cell orientation was quantified using OrientationJ [44], an ImageJ (NIH) plugin for nuclear directional analysis. To segregate images into 'along-axis' and 'off-axis' locations, a geometric analysis routine was developed to create three equal-area segmented arc-based areas between adjacent micropockets (supplemental figure 1 is available online at stacks.iop.org/BF/11/045013/mmedia).

Statistical analysis

Comparative data analysis of populations was performed without pre-specifying a required effect size. Datasets were normally distributed, with similar variances between compared groups. All statistical analysis was conducted using two-tailed one-way ANOVA analyses with Tukey post-hoc pairwise comparisons (Prism; GraphPad Software, La Jolla, CA). *P*-values less than 0.05 were considered significant.

Results and discussion

Fabrication of micropocket culture devices

3D printed templates with spherical well diameters as small as 400 μm and openings of 100 μm were readily fabricated using stereolithographic 3D printing (figure 2(a)). The micropocket dimensions, spacing, and chip size can be increased by changing the 3D

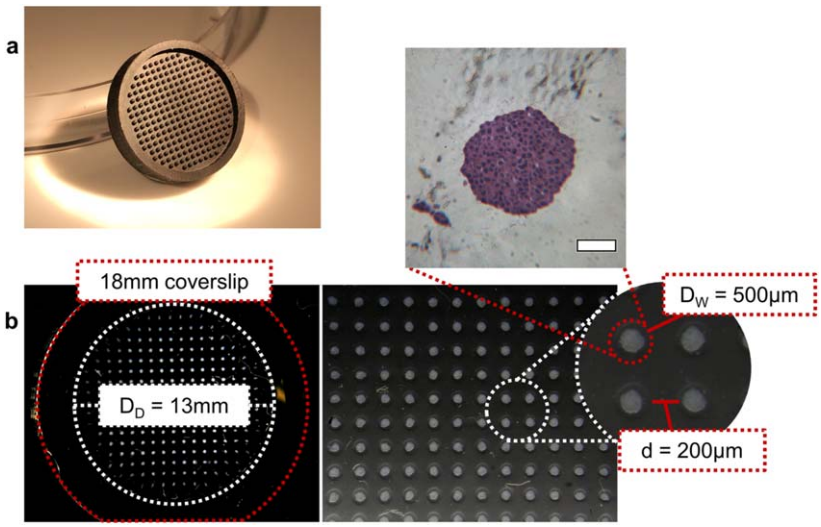

Figure 2. High-throughput formation of aggregates using hydrogel MPoC chips. (a) Prototypical 3D printed negative mold with spherical pockets in coverslip-compatible format. (b) Polyacrylamide positive molds were readily replicated on 18 mm diameter coverslips, with 13 mm device dimensions, and >200 pockets per chip when designed with MPoC diameter D_w of 500 μm and pitch of 200 μm. T-47D human epithelial ductal carcinoma cells are demonstrated here to form a well-defined array of spheroids with tight boundaries within the MPoC chip. (b, insert) Haemotoxylin and Eosin (H&E) stains of sectioned spheroids demonstrates tight packing of cells, with a defined border, indicating that T-47Ds form a tight spheroid. Spheroid structures are larger than the pocket opening, but smaller than the pocket diameter, indicating that T-47D aggregates compact within the pockets after initial seeding (scale bar = 100 μm).

print, where the primary limitations are the build area and patterning resolution of the 3D printer. For experiments described in this manuscript, negative molds with 100–220 micropockets (1000, 500, and 400 μm diameters) could each be printed on a 13 mm diameter circular plate within 20 min (figures 2(a), (b)). The device dimensions described were designed to transfer the replica-molded pattern to an 18 mm diameter coverslip, which can then be easily cultured in a standard 12-well plate.

We originally attempted to replicate prototypical reverse-tapered inverted cone structures in standard and softened formulations of polydimethylsiloxane (PDMS), a silicone rubber material commonly used in microfabricated systems. While PDMS did release cleanly from the 3D printed mold material, peeling the PDMS from the device often broke any reverse-tapered structures with anchoring dimensions of <200 μm (supplementary figure S2(a)).

Following this initial failure of a standard microfabrication material, we developed several criteria to select an appropriate alternative replica molding material. First, the material must be resistant to cell and protein adhesion, while simultaneously allowing transport of media and waste to support cell culture; suggesting that a hydrogel might be suitable. Second, the material must be sufficiently compliant to allow release from an overhanging template structure. Third, the material must retain the molded features over time in cell culture conditions, and must hence be mechanically stable and resistant to cell degradation processes. Based on these criteria, we chose to use the hydrogel polyacrylamide (PAAm) for this application, as it is natively resistant to protein adhesion [45], is stiffness-tunable [40], retains microscale features on molding [46], and retains stable, linear elastic mechanical properties even after extended time in culture [47]. Furthermore, as PAAm is commonly used in many wet labs for gel electrophoresis, the reagents are inexpensive, readily available from commercial sources and relatively easy to handle; which would reduce barriers to adoption of this technology.

We empirically selected and mechanically characterized a polyacrylamide formulation, determining that at the low strains expected for this application, the shear modulus G was ~6.5 kPa (supplemental figure S3). This is ~40× softer than standard PDMS (G ~ 250 kPa) [43], and , and was relatively easy to peel from the 3D prints without damaging the patterns (supplementary figure S2(b)). This formulation was also sufficiently rigid to (a) retain features after peeling and (b) not swell noticeably after gelation, which would affect any replicated features, and (c) retained storage and loss modulus characteristics over several days in culture (supplementary figures S3(b)–(c)), consistent with previous studies of polyacrylamide hydrogels [47].

Micropocket aggregate formation

Once seeded, cells took less than 5 min to settle into the pockets and within a day formed uniformly-sized multicellular aggregates. Polyacrylamide is well established to resist cell and protein adhesion unless explicitly modified using chemical means and hence, is an excellent 'blank slate' material to allow aggregate formation. As expected, the aggregates remained in

their micropockets after formation and during routine handling, which allowed for formation and maintenance of well-defined arrays of positioned multicellular aggregates (figure 2(b)). If desired, aggregates could be removed by jamming a pipette tip over the location and aspirating rapidly, but they could not be dislodged by accidental shaking of the cultures or during routine liquid exchanges. A histology section of a T-47D aggregate (figure 2(b), insert) reveals a tightly packed internal structure with minimal gaps, as well as a well-defined boundary [48], indicating that T-47D cell aggregates do transition towards forming tight spheroids in this culture system.

The produced aggregates are consistently smaller than the micropocket diameters, indicating that they compact after the initial seeding, consistent with previous studies [47]. Multicellular aggregates prepared in 500 μm diameter pockets (~60 nl volume), compact to approximately 250 μm diameter aggregates (~10 nl volume). Therefore, aggregates sit in ~50 nl of media within the hydrogel pocket, which would in itself be sufficient to sustain these aggregates for at least 2–3 h, given an estimated glucose consumption rate of 10^{-5} nmol glucose per cell per second (aggressively estimated as 100× greater than a fibroblast) [49], cell volume of 1 pl [50], and use of 25 mM high-glucose culture media. This simplified estimation does not account for diffusion limitations within spheroids [48], which would further reduce glucose consumption. More importantly, polyacrylamide is over 98% water [51–53] and hence allows diffusive and convective replenishment of media through the porous material. This mass transport would rapidly refresh media from the large volume well through the thin hydrogel structure, further supporting cell culture. In contrast, PDMS silicones do allow comparable levels of oxygen transport (3.51×10^5 cm^2 s^{-1} at 25 °C in PDMS [54] compared to $D = 2.2 \times 10^5$ cm^2 s^{-1} at 25 °C in polyacrylamide [55]) but do not permit equilibration of other small molecules and growth factors [17] through diffusive or convective means.

Control of multicellular aggregate size

We originally reasoned that the dimensions of multicellular aggregates could be controlled by changing pocket volumes or controlling the seeding density of cells into these devices. Hence, we tested increasing seeding concentrations of T-47D cells in 500 μm diameter pockets (figure 3(a)). Interestingly, we found that seeding density only affects the size of the produced multicellular aggregate up to a point. For seeding densities greater than 3×10^6 cells ml^{-1}, mean diameters were within 25 μm of each other, or one or two additional cell layers. These small differences were not statistically significant, even for large sample sizes of $n = 20$–30 when seeding densities were greater than 7×10^6 cells ml^{-1}. This is reasonable to expect, if we consider that over the settling time, the pockets can be 'filled' with loosely packed and roughly spherical non-adhered cells that prevent the entry of additional cells. Then, over a timescale of hours, the loosely-packed cells deform to produce compacted aggregates. These results are particularly important in that devices are seeded with sufficiently high cell densities will produce uniformly-sized aggregates, thereby reducing the need for precise counting and day-to-day consistency required for other aggregation culture techniques.

Using a baseline seeding density of 5×10^6 cells ml^{-1}, we then characterized three breast cancer cell lines in two micropocket diameters in our culture platform. Human breast cancer cell lines MDA-MB-231, MCF-7, and T-47D cells, which together account for 2/3 of all submitted breast cancer-related abstracts on the MEDLINE database [56], were found to form consistently sized aggregates in the MPoC devices based on micropocket dimensions. Across all cell types, 400 μm diameter micropockets produced aggregates of between 125 and 200 μm diameter, while larger 1 mm diameter micropockets produced aggregates of 300–400 μm in diameter. Cell type had a large effect on multicellular aggregate size distribution, with T-47D aggregates exhibiting tight size distribution across samples, while the other cells exhibited greater variability. This is likely due to differences in the way distinct cell types act to compact the aggregate. Variations in intrinsic cell size and incomplete filling of larger pocket dimensions at this seeding density (optimized for T-47D cells in 500 μm diameter pockets) may also contribute to the observed variability. Hence, if aggregate size is a critically important parameter for the intended application, a cell density seeding optimization curve would need to be performed for each cell type and pocket size.

To determine whether MPoC chips are forming sphere-like structures, we quantified the circularity of the produced aggregates (figure 3(c)). We defined circularity as the ratio between the measured perimeter and the theoretical perimeter for a perfect circle of equivalent area. Some variability was observed based on cell type. The circularity of T-47Ds approached that of a perfect circle consistently across all measured samples, while MDA-MB-231 and MCF-7 lines showed greater variability. This is consistent with the idea that T-47Ds aggregates compact tightly to form spheroids, suggested by the decreased aggregate size (figure 3(b)) and the well-defined aggregate border (figure 2(b); figure 5(b)); while the other cell types form less tightly compacted structures.

Integrated labeling, treatment and analysis directly on chip

A critical advantage of the partially-closed micropocket design is that samples can be washed repeatedly without sample loss, as they remain immobilized in the porous device. This greatly facilitates imaging and

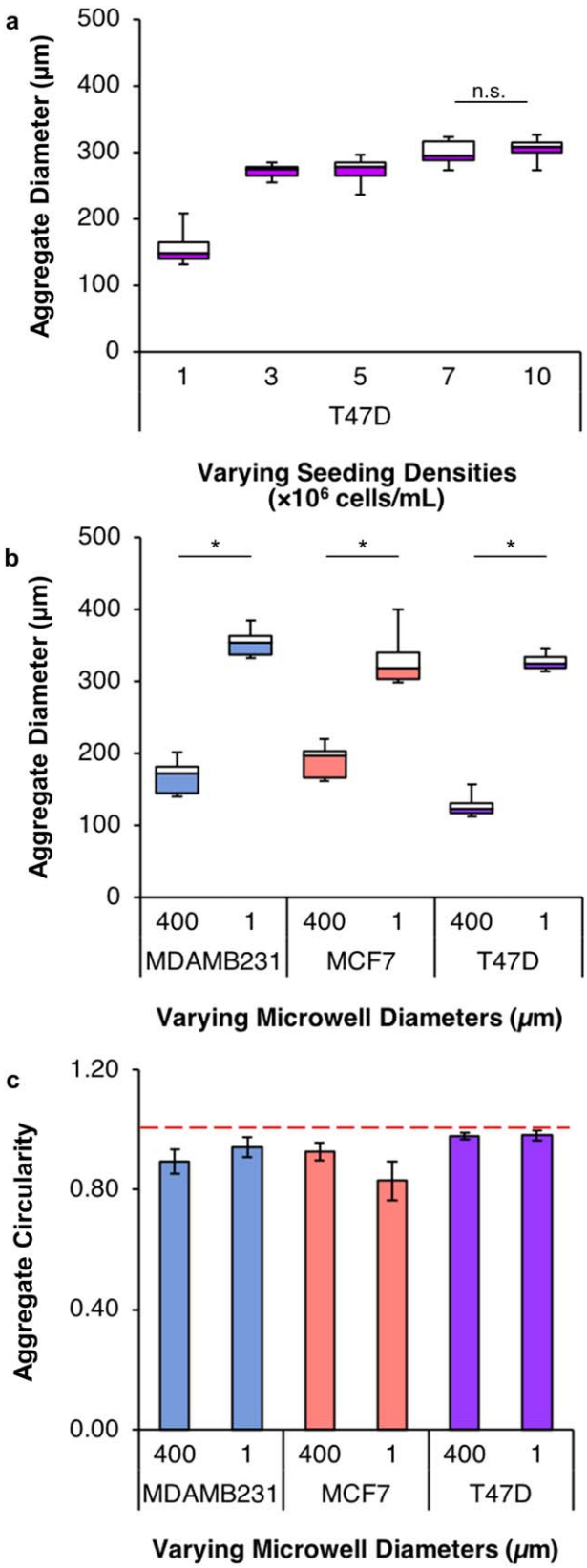

Figure 3. Characterization of multicellular aggregate size and shape in MPoC chips. (a) Aggregate dimensions are independent of cell seeding density beyond a certain threshold. T-47D spheroids were formed in 500 μm diameter pockets by seeding devices with 1, 3, 5, 7 and 10 $\times$ 10^6 cells ml^{-1} of culture media (n = 21–30, n.s. $p > 0.05$). (b) Pocket dimensions can be designed to control aggregate diameters. MDA-MB-231, MCF-7, and T-47D cells were seeded in 400 μm pocket diameters and 1 mm pocket diameter devices with 100 μl of a 5 $\times$ 10^6 cells ml^{-1} cell suspension. Pocket diameters significantly affected aggregate dimensions (n = 30, $^*p < 0.0001$; box plots indicate median, first-to-third quartile, and range). (c) Measurement of circularity of MDA-MB-231, MCF-7, and T-47D aggregates demonstrates that T-47D form the most circular spheroids in both 400 μm and 1 mm diameter pockets (mean +/− standard deviation, n = 30; red dashed line indicates a perfect circle).

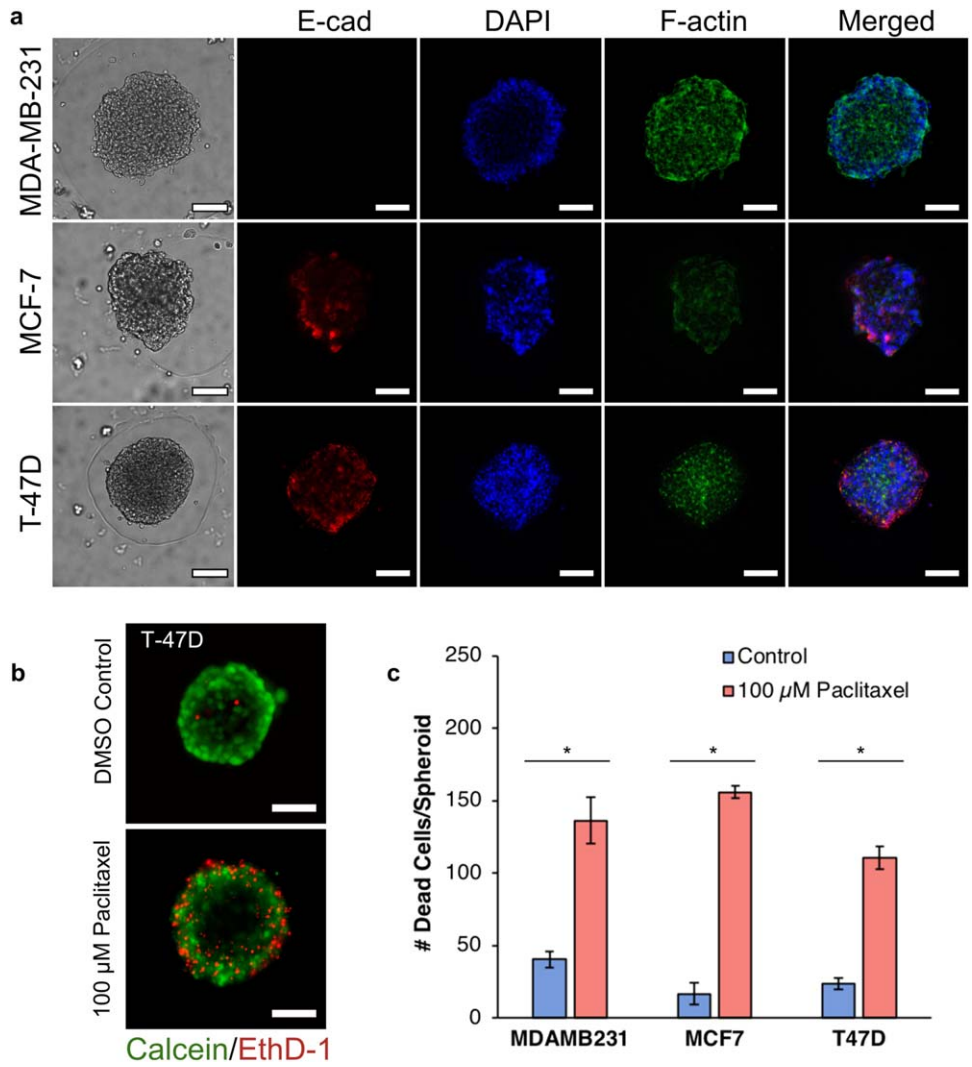

Figure 4. MPoC platform enables integrated labeling and stimulation of cell aggregates directly on chip. (a) Multiple wash steps required for fluorescent immunostaining and imaging do not dislodge aggregates from within the pockets, which also allow sufficient transport of large antibodies for labeling. E-cadherin (red), nuclear DAPI (blue) and F-actin (green). MDA-MB-231 cells display no discernible E-cadherin, and well-defined F-actin structures, while T-47D cells express organized E-cadherin on the spheroid periphery and punctate actin structures. (b) Representative images of live/dead stains of whole T-47D spheroids following treatment with vehicle control or 100 μM paclitaxel for two days. (scale bar $=$ 100 μm) (c) Number of dead cells per spheroid vary depending on cell type and paclitaxel treatment (data presented as mean $+/-$ standard deviation, $n = 5$, $^{*}p < 0.05$).

analysis. To demonstrate this capability, we performed an indirect immunostain for E-cadherin and F-actin/nuclei directly on chip. The standard indirect immunostaining protocol requires 18 liquid exchanges including multiple wash steps (see Methods) and is hence, challenging to perform on systems that have even a small loss rate of samples per wash step. After aggregation for 24 h, MPoCs were fixed, permeabilized, and labeled as described. The staining procedure did not cause any sample losses, which could then be imaged directly on chip (figure 4(a)). In this example, MDA-MB-231 cells did not express detectable E-cadherin levels, while E-cadherin was observed in MCF-7 cells and organized around the aggregate boundary in T-47D cells, consistent with the formation of tight borders associated with spheroids [48, 57]. This is consistent with previous literature reports [58, 59]. F-actin images were also obtained and showed a clearly-defined architecture in the mechanically active MDA-MB-231 cells and a more punctate actin morphology in the compacted MCF-7 and T-47D lines, consistent with other studies [57].

To demonstrate the ability to test target therapeutic compounds in culture, we conducted a simple cytotoxicity drug test and monitored cell viability with a fluorescent live/dead stain. Aggregates of all three cell types were formed for 48 h and treated with 100 μM paclitaxel or a vehicle control in complete media for 24 h, before the live/dead assay. As expected, paclitaxel induces cell death in the spheroids and this was easily observed as a greatly increased number of red dead cells (figure 4(b)). A disruption of the tight boundary surrounding the aggregate can also be observed when treating T-47D aggregates with paclitaxel. Counting the number of dead cells after treatment demonstrated a significant increase in cell death

with paclitaxel (figure 4(c)), demonstrating the potential applicability of this platform in drug testing and screening applications. Interestingly, the number of dead cells caused by this concentration of paclitaxel was not as high as expected based on LD50 curves established for 2D cultures, but this is expected as culture of cancer cells in 3D aggregates has been shown to enhance cytotoxic resistance to these drugs [60–62].

Taken together, these experiments demonstrate the ease with which biological samples can be labeled and treated, without loss of precious sample materials during the multiple liquid exchange steps required for each of these procedures. Furthermore, the ability to stain and image directly on chip makes repeated analysis of the same aggregate substantially easier, as the aggregate position is maintained during all sample manipulations, allowing the use of automated stage positioning microscopy techniques. This platform may hence have broad applicability in many areas of aggregate-based biological discovery.

Comparison of aggregate formation against other technologies

We sought to benchmark our technology against two other technological approaches to forming aggregates in terms of applicability to various cell types. We compared our system with hanging drop cultures, which prevent cells from attaching to any other surface, and is hence similar in mechanism of action to pipette-able hanging drop plates [63] and non-adhesive microwells [21, 36]; and to an aqueous two-phase bioprinting strategy [19, 20], in which cells are physically confined close to each other, and can be considered similar in mechanism to microcavity-based strategies [27] (figure 5(a)). Both strategies have proven advantages for spheroid culture, most notably the ability to individually stimulate each spheroid individually, as they are separated by a physical barrier. This advantage comes with a major limitation in that hanging-drop plates and ATPS printing techniques can at best be scaled to the density of a 1536-well plate (2.3 mm center-to-center pitch) [64] and requires multiple pipetting steps to operate. In contrast, the MPoC devices are not suitable for individually assayable spheroid formation, but readily achieve a pitch of 0.7 mm, and can hence produce aggregates with an ~10.8-fold increase in areal density (~0.5 mm^2/aggregate, compared to ~5.3 mm^2/aggregate). The MPoC densities reported here are similar to those that can be achieved with single-layer microfluidic devices [31, 65] or uncontrolled aggregation in arrayed structures such as agar-based microwell platforms [36, 66], which are amongst the highest-throughput aggregation technologies available today.

We tested each of these techniques against MPoC chips with MDA-MB-231, MCF-7, and T-47D cell lines (representative results in figure 5(b)). The hanging drop method tended to produce highly fenestrated structures in 231 and T-47D cells, and poorly compacted structures in MCF-7 cells. The ATPS systems consistently produced uniform 231 aggregates, but highly deformed and fenestrated structures in MCF-7 and T-47D lines. In contrast, the MPoC technique produced spherical, compacted, organized aggregates with varying degrees of boundary tightness in all three cell lines, with high reproducibility and consistency (figure 5(b)). It should be noted that media formulation may play an important role in whether or not aggregate structures form in certain cell types [34, 48]. In this study we did not optimize media for any of the specific techniques, and instead used the standard media formulation 'as is' for all three comparisons. Hence, while each of these techniques may be tuned to produce spheroids, the MPoC platform eliminated the need for such optimization.

Anecdotally, in addition to testing multiple cell types, we have also put MPoC chips in the hands of multiple users with varying degrees of microfabrication and cell culture training, and all have reported highly consistent and easy aggregate formation in their hands, with minimal experimental variation and sample loss. Speculatively, we believe that the MPoC platform successfully forms aggregates in a wide variety of cells because the cells are loosely but consistently filled into the micropockets, which constrains the cells into a configuration that requires them to compact uniformly. Furthermore, the porous hydrogel structure ensures that the aggregates compact in a nutrient-rich environment with minimal diffusive limitations, which could also contribute to the success rates observed [19].

MPoC supported production of embedded aggregate-based tissues

To further demonstrate the versatility of the MPoC platform beyond aggregate formation and analysis which can be achieved to varying degrees with other techniques, we tested additional tissue processing steps that could enable production of engineered tissues with precise positional control over embedded aggregates. As a general strategy, placing aggregates in 3D tissues has previously been used to construct functional and implantable liver tissues [14], model cancer microenvironments [15], and for drug discovery applications [67], and hence could be of broad utility. Here, we propose aspirating the culture media from MPoC chips and replacing it with a natural hydrogel prepolymer, such as collagen, allows the spatially patterned aggregates to invade into the matrix and interact with other closely-positioned aggregates (figure 6(a)).

We tested this approach by embedding arrays of aggregates in collagen, and confirmed that aggregates were encapsulated in the collagen matrix by physically peeling away the collagen gel after it polymerized. The

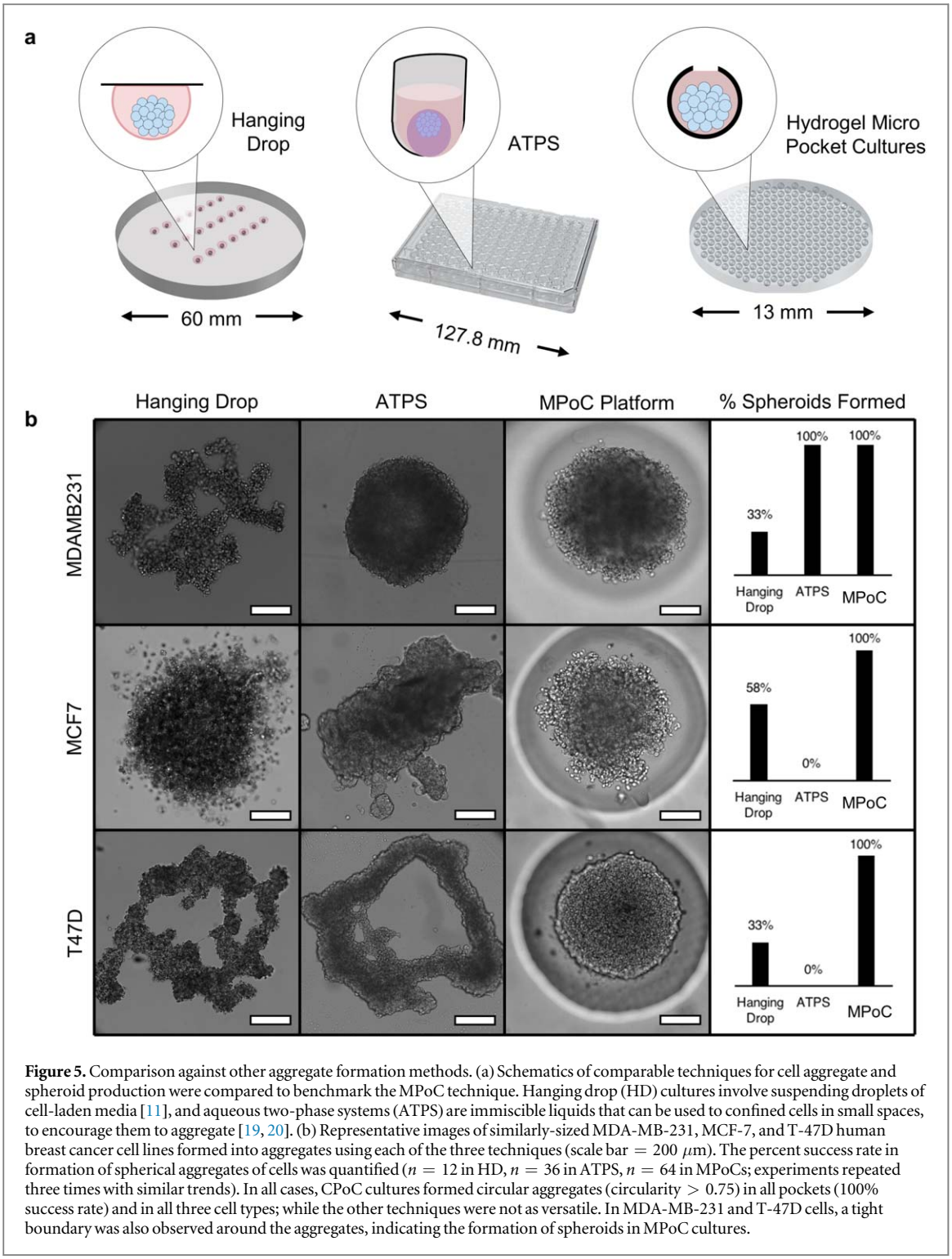

Figure 5. Comparison against other aggregate formation methods. (a) Schematics of comparable techniques for cell aggregate and spheroid production were compared to benchmark the MPoC technique. Hanging drop (HD) cultures involve suspending droplets of cell-laden media [11], and aqueous two-phase systems (ATPS) are immiscible liquids that can be used to confined cells in small spaces, to encourage them to aggregate [19, 20]. (b) Representative images of similarly-sized MDA-MB-231, MCF-7, and T-47D human breast cancer cell lines formed into aggregates using each of the three techniques (scale bar $= 200\ \mu$m). The percent success rate in formation of spherical aggregates of cells was quantified ($n = 12$ in HD, $n = 36$ in ATPS, $n = 64$ in MPoCs; experiments repeated three times with similar trends). In all cases, CPoC cultures formed circular aggregates (circularity > 0.75) in all pockets (100% success rate) and in all three cell types; while the other techniques were not as versatile. In MDA-MB-231 and T-47D cells, a tight boundary was also observed around the aggregates, indicating the formation of spheroids in MPoC cultures.

multicellular aggregates were transferred from the MPoC device into the collagen gel, where they maintained their arrayed positions, confirming that collagen enters the micropocket and surrounds the aggregate. If desired at this stage, gels could also be back-filled with collagen at this stage to create fully embedded and positioned aggregates as has previously been done [14]. We then confirmed contact between the gel and the aggregates by monitoring destabilization of the aggregates and invasion into the surrounding matrix, in response to stimulatory factors, TGF-β1 and HGF, known to be associated with cell migration [68, 69] and tumor invasion in breast tissue [70, 71] (figure 6(b)). T-47D cells remained tightly aggregated after 48 h in embedded culture, even when stimulated with TGF-β1 or HGF (consistent with literature reports [72]). In contrast, MDA-MB-231 cells displayed spontaneous aggregate disruption and invasion into the collagen matrix. This effect was enhanced by the addition of HGF, resulting in larger invasion areas (figure 6(b)). These images confirm that aggregates are embedded within a matrix, and remain viable and

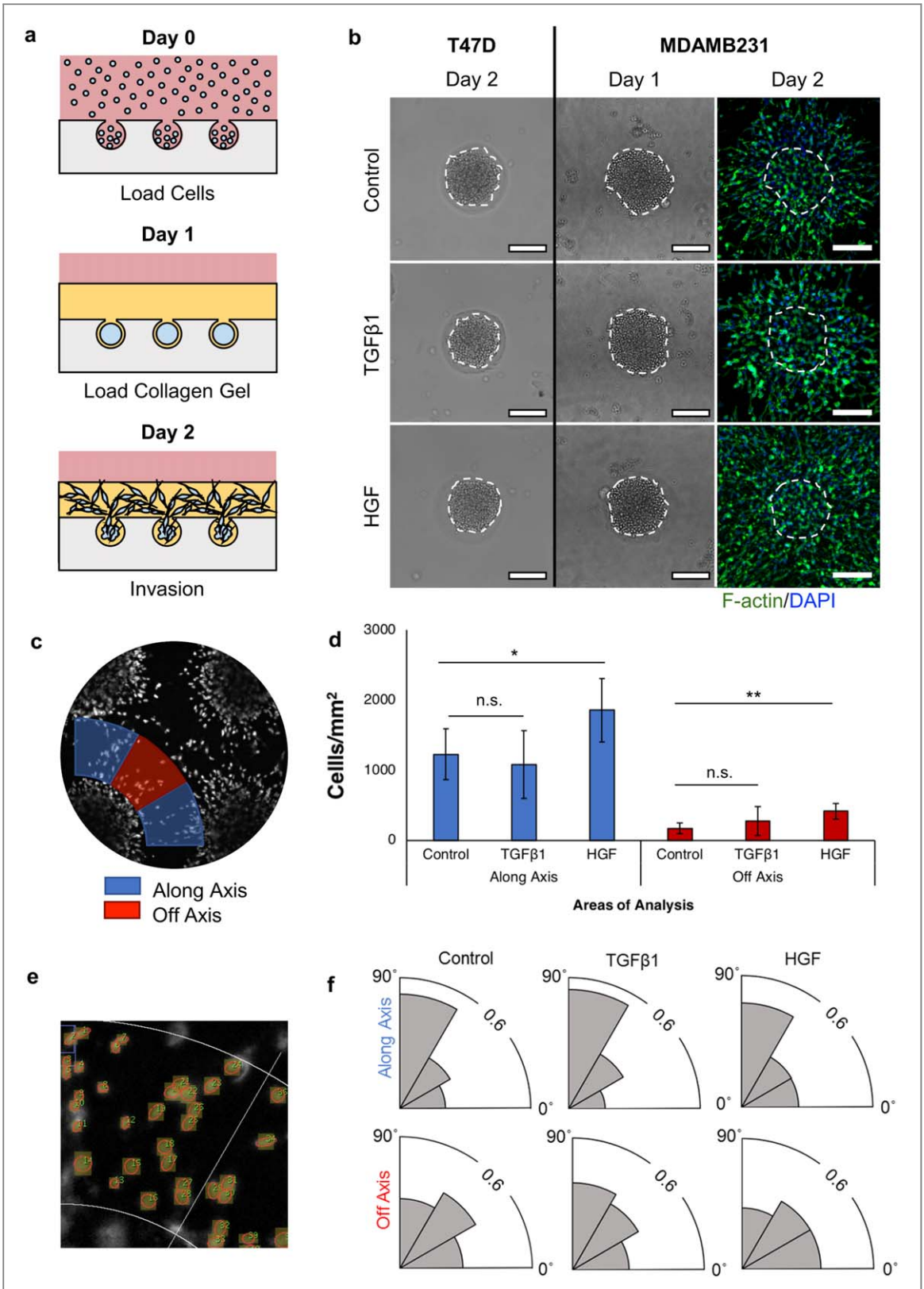

Figure 6. Positioned spheroids can be embedded in extracellular matrix material to form micropatterned tissues for analysis of invasion. (a) Schematic of collagen invasion assay, in which collagen is loaded onto the MPoC surface and gelled to provide a material into which the aggregated cells can invade. (b) While T-47D cells did not substantially invade into the surrounding collagen even under external stimulation with TGF-β1 or HGF, MDA-MB-231 cells invaded readily into the surrounding tissue in basal medium. This effect was enhanced with the addition of HGF, but not TGF-β1 (scale bars $= 200\ \mu$m). (c), (d) Cells leave aggregates and invade directionally towards other nearby aggregates. (c) Regions of interest are defined as either 'along axis' between spheroids, or 'off-axis', to examine (d) cell density after two days of invasion with and without stimulation, which showed significantly greater 'along-axis' density compared to 'off-axis', and with HGF stimulation. (e), (f) Cellular orientation during invasion was assessed using (e) nuclear axial orientation in (f) the along-axis or off-axis regions of culture. Cells preferentially oriented towards other aggregates during invasion. (Data presented as mean $+/-$ standard deviation, $n = 5$, $^{*}p < 0.05$, $^{**}p < 0.01$, n.s. $p > 0.05$.)

responsive to soluble signals delivered through the surrounding collagen gel.

Analysis of migration between precisely-positioned aggregates

We then asked whether spatial positioning of aggregates can play a role in enhancing migration and invasive behavior. Cells can sense and migrate along gradients of soluble and matrix-bound signals [73], or mechanical deformations in the matrix caused by other cells [74–76]. To determine if nearby aggregates might influence the behavior of invading cells, we cultured aggregates in square patterns, such that the distance between adjacent aggregates is ~1.4× less than the distance between diagonally opposite aggregates. We termed these lines 'along-axis' and 'off-axis' respectively (figure 6(c); supplementary figure S1), and quantified the areal density of cells in these regions (figure 6(d)). Areas along the axis between two adjacent aggregates were significantly more densely populated than areas between diagonally separated aggregates; and this effect in both along-axis and off-axis regions was significantly enhanced by stimulation with HGF, but not by TGF-β1. These results demonstrate that invasive cells preferentially migrate towards surrounding aggregates.

To further confirm that cells are undergoing directional invasion, the orientation of the cells was assessed relative to the axis along which they are positioned (figure 6(e)). Cells in the highly populated 'along axis' region preferentially aligned along the shortest distance between aggregates (figure 6(f)) indicating that cells do actively sense and migrate towards adjacent aggregates. No changes to this orientation were observed with TGF-β1 stimulation, but the fraction of cells exhibiting this orientation decreased when stimulated with HGF. This indicates that HGF induces non-directional scattering, overriding directional cues provided by a nearby aggregate. No significant orientation was observed 'off-axis', suggesting that the off-axis distance, is too far to establish a signaling or mechanical gradient needed for directional cell migration, when compared with the closer adjacent aggregates. Hence, substantial differences exist in cell orientation and migration based on positioning differences of less than 200 μm, emphasizing the critical need for patterning technologies capable of positioning aggregates with high spatial resolution and repeatability.

Taken together, these results demonstrate an all-in-one strategy to form, embed, treat, and monitor complex engineered tissues, using a simple and robust handling methodology.

Current technical limitations

The MPoC platform described here does present a few limitations in engineering tissues. First, the overhanging structures required on the master molds are most easily achieved using a 3D printer, which presents some challenges. Although better than fused-deposition modeling printing, the stereolithographic light-based printers used here presents size and resolution limitations which sets a lower limit on the density of aggregates achievable and on the smallest aggregate size. Since the spheroids produced here are comparable in size to most used in the literature, producing smaller aggregates will require alternative and less widely accessible microfabrication processes such as femtosecond-laser 3D printing [77] or shrinking of patterned scaffolds [78].

Second, a large number of cells are needed to achieve the high seeding densities required for the uniform spheroid production regime described here. While this is not a concern for cell lines, adapting this platform for limited primary cells will require some modifications, such as a funnel structure to feed a small volume of cell suspension into a single well [30]. Although this would increase device complexity and would require a pipetting step for each spheroid, it would enable production of spheroids from precious cell material. To this end, one can envision a molding system that allows production of cavities in gels polymerized directly into glass-bottom micro-well dishes, as has been previously demonstrated for flat polyacrylamide gels [79].

Third, although the standard formulation of polyacrylamide used here was suitable for our needs, polyacrylamide is a relatively brittle gel that may not be compatible with advanced applications, such as when mechanical deformation must be applied to the tissues being produced. More recent hydrogel formulations such as interpenetrating networks of polyacrylamide and alginate [80, 81] may be used to dramatically improve these mechanical properties for such applications; and exploring these alternative hydrogel material systems would be of considerable interest in providing better control over hydrogel structure, or even incorporating smart responsive behaviour to environmental cues.

Finally, the described technique for 3D tissue formation is currently only applicable to either a single cell type, or to homogenously mixed cell populations. Positioning aggregates of different compositions at precise locations would require additional structures to block access of cells to certain pockets and form aggregates sequentially on a per-pocket basis.

Conclusions

The core innovation leveraged here for the simultaneous formation of multiple, multicellular aggregates at defined positions on a device is that of a passive, size-based, one-way valve; a partially-closed pocket structure that allows individual cells to enter a cavity, but does not allow them to leave once they form an aggregate. These microscale pockets can be fabricated in polyacrylamide hydrogels using broadly-accessible

and user-friendly 3D printing and replication strategies and positioned as desired to form dense arrays of uniform cell aggregates. This general strategy provides an extremely simple and readily-adoptable strategy to produce uniformly-sized multicellular aggregates in a high-throughput format. Critically, this strategy also allows easy handling without undesired loss of samples, allowing robust labeling, treatment, and analysis directly on chip. The use of polyacrylamide hydrogels was particularly important to support these applications, as we empirically determined that the mechanical characteristics of the hydrogel are suitable for replica-molding reverse-tapered structures, the material prevents undesired cell binding to allow aggregate formation, and allows maintenance of cell cultures via diffusive and convective mass transport through the porous hydrogel material. Together, these properties enable the formation of aggregates in cell lines that are not as amenable to aggregation using other techniques. Finally and uniquely, this platform can also be used as an all-in-one solution to form spheroids, and then transfer them into an embedding material, enabling fabrication of tissues with precise positioning between embedded aggregates. We demonstrate the utility of these produced tissues as a platform to study cellular invasion. We observed that migration of certain cell types can be strongly biased towards nearby aggregates and that the relative distances between aggregates and soluble stimulation were critical parameters in directing this movement. More broadly, this strategy to produce positioned and embedded aggregates in tissues may be applied to a wide variety of tissue-engineering related fields that require aggregate formation as a critical processing step.

Acknowledgments

This work was supported by the Canadian Cancer Society (Grant # 704422), FRQNT Team grant (205292), NSERC Discovery RGPIN-2015-05512, and the Canada Research Chairs program in Advanced Cellular Microenvironments to CM.

ORCID iDs

Stephanie Mok https://orcid.org/0000-0003-1700-0157
Christopher Moraes https://orcid.org/0000-0002-8950-2212

References

[1] Sutherland R M, McCredie J A and Inch W R 1971 Growth of multicell spheroids in tissue culture as a model of nodular carcinomas *JNCI J. Natl Cancer Inst.* **46** 113–20
[2] Sutherland R M 1988 Cell and environment interactions in tumor microregions: the multicell spheroid model *Science* **240** 177–84
[3] Gong X *et al* 2015 Generation of multicellular tumor spheroids with microwell-based agarose scaffolds for drug testing *PLoS One* **10** e0130348
[4] Kim C, Bang J H, Kim Y E, Lee S H and Kang J Y 2012 On-chip anticancer drug test of regular tumor spheroids formed in microwells by a distributive microchannel network *Lab Chip* **12** 4135–42
[5] Grimshaw M J *et al* 2008 Mammosphere culture of metastatic breast cancer cells enriches for tumorigenic breast cancer cells *Breast Cancer Res.* **10** R52
[6] Shaw F L *et al* 2012 A detailed mammosphere assay protocol for the quantification of breast stem cell activity *J. Mammary Gland Biol. Neoplasia* **17** 111–7
[7] Choi Y Y *et al* 2010 Controlled-size embryoid body formation in concave microwell arrays *Biomaterials* **31** 4296–303
[8] Cha J M *et al* 2015 Embryoid body size-mediated differential endodermal and mesodermal differentiation using polyethylene glycol (PEG) microwell array *Polym. Soc. Korea* **23** 245–55
[9] Dong G *et al* 2019 Serum-free culture system for spontaneous human mesenchymal stem cell spheroids formation *Cell Biol.* (https://doi.org/10.1101/666313)
[10] Kunz-Schughart L A, Freyer J P, Hofstaedter F and Ebner R 2004 The use of 3D cultures for high-throughput screening: the multicellular spheroid model *J. Biomol. Screen.* **9** 273–85
[11] Tung Y-C *et al* 2011 High-throughput 3D spheroid culture and drug testing using a 384 hanging drop array *Analyst* **136** 473–8
[12] Chen Y-C, Lou X, Zhang Z, Ingram P and Yoon E 2015 High-throughput cancer cell sphere formation for characterizing the efficacy of photo dynamic therapy in 3D cell cultures *Sci. Rep.* **5** 12175
[13] Hou S *et al* 2018 Advanced development of primary pancreatic organoid tumor models for high-throughput phenotypic drug screening *SLAS Discovery Adv. Life Sci. R&D* **23** 574–84
[14] Stevens K R *et al* 2013 InVERT molding for scalable control of tissue microarchitecture *Nat. Commun.* **4** 1847
[15] Tevis K M, Colson Y L and Grinstaff M W 2017 Embedded spheroids as models of the cancer microenvironment *Adv. Biosyst.* **1** 1700083
[16] Foty R 2011 A simple hanging drop cell culture protocol for generation of 3D spheroids *J. Vis. Exp.* **51** e2720
[17] Moraes C, Simon A B, Putnam A J and Takayama S 2013 Aqueous two-phase printing of cell-containing contractile collagen microgels *Biomaterials* **34** 9623–31
[18] Han C, Takayama S and Park J 2015 Formation and manipulation of cell spheroids using a density adjusted PEG/DEX aqueous two phase system *Sci. Rep.* **5** srep11891
[19] Atefi E, Lemmo S, Fyffe D, Luker G D and Tavana H 2014 High throughput, polymeric aqueous two-phase printing of tumor spheroids *Adv. Funct. Mater.* **24** 6509–15
[20] Ham S L, Atefi E, Fyffe D and Tavana H 2015 Robotic production of cancer cell spheroids with an aqueous two-phase system for drug testing *J. Vis. Exp.* **98** e52754
[21] Ungrin M D, Joshi C, Nica A, Bauwens C and Zandstra P W 2008 Reproducible, ultra high-throughput formation of multicellular organization from single cell suspension-derived human embryonic stem cell aggregates *PLoS One* **3** e1565
[22] Glicklis R, Merchuk J C and Cohen S 2004 Modeling mass transfer in hepatocyte spheroids via cell viability, spheroid size, and hepatocellular functions *Biotechnol. Bioeng.* **86** 672–80
[23] Yuan X, Tsai A-C, Farrance I, Rowley J A and Ma T 2018 Aggregation of culture expanded human mesenchymal stem cells in microcarrier-based bioreactor *Biochem. Eng. J.* **131** 39–46
[24] Singh M, Close D A, Mukundan S, Johnston P A and Sant S 2015 Production of uniform 3D microtumors in hydrogel microwell arrays for measurement of viability, morphology, and signaling pathway activation *Assay Drug Dev. Technol.* **13** 570–83
[25] Ivanov D P and Grabowska A M 2017 *In vitro* tissue microarrays for quick and efficient spheroid characterization *SLAS Discovery Adv. Life Sci. R&D* (https://doi.org/10.1177/2472555217740576)

[26] Goral V N, Au S H, Faris R A and Yuen P K 2014 Microstructured multi-well plate for three-dimensional packed cell seeding and hepatocyte cell culture *Biomicrofluidics* **8** 046502

[27] Hsiao A Y *et al* 2009 Microfluidic system for formation of PC-3 prostate cancer co-culture spheroids *Biomaterials* **30** 3020–7

[28] Bertillot F *et al* 2017 Microfluidic-based generation of 3D collagen spheres to investigate multicellular spheroid invasion *3D Cell Culture* pp 269–79(New York, NY: Humana Press)

[29] Ong L *et al* 2017 A 3D printed microfluidic perfusion device for multicellular spheroid cultures *Biofabrication* **9** 045005

[30] Marimuthu M *et al* 2018 Multi-size spheroid formation using microfluidic funnels *Lab Chip* **18** 304

[31] Moshksayan K *et al* 2018 Spheroids-on-a-chip: recent advances and design considerations in microfluidic platforms for spheroid formation and culture *Sensors Actuators* B **263** 151–76

[32] Sackmann E K, Fulton A L and Beebe D J 2014 The present and future role of microfluidics in biomedical research *Nature* **507** 181–9

[33] Sant S and Johnston P A 2017 The production of 3D tumor spheroids for cancer drug discovery *Drug Discovery Today Technol.* **23** 27–36

[34] Froehlich K *et al* 2016 Generation of multicellular breast cancer tumor spheroids: comparison of different protocols *J. Mammary Gland Biol. Neoplasia* **21** 89–98

[35] Cui X, Hartanto Y and Zhang H 2017 Advances in multicellular spheroids formation *J. R. Soc. Interface* **14** 20160877

[36] Futrega K *et al* 2015 The microwell-mesh: a novel device and protocol for the high throughput manufacturing of cartilage microtissues *Biomaterials* **62** 1–12

[37] Kandow C E, Georges P C, Janmey P A and Beningo K A 2007 Polyacrylamide hydrogels for cell mechanics: steps toward optimization and alternative uses *Methods in Cell Biology* vol 83 (New York : Academic) pp 29–46

[38] Caliari S R and Burdick J A 2016 A practical guide to hydrogels for cell culture *Nat. Methods* **13** 405–14

[39] Yuk H, Zhang T, Lin S, Parada G A and Zhao X 2016 Tough bonding of hydrogels to diverse non-porous surfaces *Nat. Mater.* **15** 190–6

[40] Tse J R and Engler A J 2010 Preparation of hydrogel substrates with tunable mechanical properties *Current Protocols in Cell Biology* ed J S Bonifacino *et al* (New York: Wiley) (https://doi.org/10.1002/0471143030.cb1016s47)

[41] Exon J H 2006 A review of the toxicology of acrylamide *J. Toxicol. Environ. Health* B **9** 397–412

[42] Smith E A and Oehme F W 2011 Acrylamide and polyacrylamide: a review of production, use, environmental fate and neurotoxicity *Rev. Environ. Health* **9** 215–28

[43] Moraes C, Labuz J M, Shao Y, Fu J and Takayama S 2015 Supersoft lithography: candy-based fabrication of soft silicone microstructures *Lab on a Chip* **15** 3760–5

[44] Püspöki Zsuzsanna, Storath Martin, Sage Daniel and Unser Michael 2016 Transforms and Operators for Directional Bioimage Analysis: A Survey *Focus on Bio-Image Informatics* (Berlin: Springer) pp 69–93

[45] Fiddes L K, Chan H K C, Lau B, Kumacheva E and Wheeler A R 2010 Durable, region-specific protein patterning in microfluidic channels *Biomaterials* **31** 315–20

[46] Charest J M, Califano J P, Carey S P and Reinhart-King C A 2012 Fabrication of substrates with defined mechanical properties and topographical features for the study of cell migration *Macromol. Biosci.* **12** 12–20

[47] Lee W *et al* 2019 Dispersible hydrogel force sensors reveal patterns of solid mechanical stress in multicellular spheroid cultures *Nat. Commun.* **10**

[48] Leung B M, Lesher-Perez S C, Matsuoka T, Moraes C and Takayama S 2015 Media additives to promote spheroid circularity and compactness in hanging drop platform *Biomater. Sci.* **3** 336–44

[49] Flamholz A, Phillips R and Milo R 2014 The quantified cell *Mol. Biol. Cell* **25** 3497–500

[50] Milo R, Phillips R and Orme N 2016 *Cell Biology by the Numbers* (New York: Garland Science)

[51] Ahmed E M 2015 Hydrogel: preparation, characterization, and applications: a review *J. Adv. Res.* **6** 105–21

[52] Hoffman A S 2012 Hydrogels for biomedical applications *Adv. Drug Deliv. Rev.* **64** 18–23

[53] Zhu J and Marchant R E 2011 Design properties of hydrogel tissue-engineering scaffolds *Expert Rev. Med. Devices* **8** 607–26

[54] Cox M E and Dunn B 1986 Oxygen diffusion in poly(dimethyl siloxane) using fluorescence quenching: I. Measurement technique and analysis *J. Polym. Sci.* A **24** 621–36

[55] Ferrell R T and Himmelblau D M 1967 Diffusion coefficients of nitrogen and oxygen in water *J. Chem. Eng. Data* **12** 111–5

[56] Lacroix M and Leclercq G 2004 Relevance of breast cancer cell lines as models for breast tumours: an update *Breast Cancer Res. Treat.* **83** 249–89

[57] Smyrek I *et al* 2019 E-cadherin, actin, microtubules and FAK dominate different spheroid formation phases and important elements of tissue integrity *Biol. Open* **8** bio037051

[58] Iglesias J M *et al* 2013 Mammosphere formation in breast carcinoma cell lines depends upon expression of E-cadherin *PLoS One* **8** e77281

[59] Chao Y L, Shepard C R and Wells A 2010 Breast carcinoma cells re-express E-cadherin during mesenchymal to epithelial reverting transition *Mol. Cancer* **9** 179

[60] Leung B M *et al* 2015 Microscale 3D collagen cell culture assays in conventional flat-bottom 384-well plates *J. Lab. Autom.* **20** 138–45

[61] Imamura Y *et al* 2015 Comparison of 2D- and 3D-culture models as drug-testing platforms in breast cancer *Oncol. Rep.* **33** 1837–43

[62] Breslin S and O'Driscoll L 2016 The relevance of using 3D cell cultures, in addition to 2D monolayer cultures, when evaluating breast cancer drug sensitivity and resistance *Oncotarget* **7** 45745–56

[63] Tung Y-C *et al* 2011 High-throughput 3D spheroid culture and drug testing using a 384 hanging drop array *Analyst* **136** 473

[64] Gutzweiler L *et al* 2017 Large scale production and controlled deposition of single HUVEC spheroids for bioprinting applications *Biofabrication* **9** 025027

[65] Kwak B, Lee Y, Lee J, Lee S and Lim J 2018 Mass fabrication of uniform sized 3D tumor spheroid using high-throughput microfluidic system *J. Control. Release* **275** 201–7

[66] Ungrin M D, Joshi C, Nica A, Bauwens C and Zandstra P W 2008 Reproducible, ultra high-throughput formation of multicellular organization from single cell suspension-derived human embryonic stem cell aggregates *PLoS One* **3**

[67] Charoen K M, Fallica B, Colson Y L, Zaman M H and Grinstaff M W 2014 Embedded multicellular spheroids as a biomimetic 3D cancer model for evaluating drug and drug-device combinations *Biomaterials* **35** 2264–71

[68] Melzer C, Ohe J, von der, Hass R and Ungefroren H 2017 TGF-β-dependent growth arrest and cell migration in benign and malignant breast epithelial cells are antagonistically controlled by Rac1 and Rac1b *Int. J. Mol. Sci.* **18**

[69] Lin F, Zhang H, Huang J and Xiong C 2018 Substrate stiffness coupling TGF-β1 modulates migration and traction force of MDA-MB-231 human breast cancer cells *in vitro ACS Biomater. Sci. Eng.* **4** 1337–45

[70] Parr C, Watkins G, Mansel R E and Jiang W G 2004 The hepatocyte growth factor regulatory factors in human breast cancer *Clin. Cancer Res.* **10** 202–11

[71] Nagaraju S, Truong D, Mouneimne G and Nikkhah M 2018 Microfluidic tumor-vascular model to study breast cancer cell invasion and intravasation *Adv. Healthcare Mater.* **7** e1701257

[72] Castro N E and Lange C A 2010 Breast tumor kinase and extracellular signal-regulated kinase 5 mediate Met receptor signaling to cell migration in breast cancer cells *Breast Cancer Res.* **12** R60

[73] Kojima T, Moraes C, Cavnar S P, Luker G D and Takayama S 2015 Surface-templated hydrogel patterns prompt matrix-dependent migration of breast cancer cells towards chemokine-secreting cells *Acta Biomater.* **13** 68–77
[74] Baker B M *et al* 2015 Cell-mediated fibre recruitment drives extracellular matrix mechanosensing in engineered fibrillar microenvironments *Nat. Mater.* advance online publication (https://doi.org/10.1038/nmat4444)
[75] Cóndor M *et al* 2019 Breast cancer cells adapt contractile forces to overcome steric hindrance *Biophys. J.* **116** 1305–12
[76] Miyazaki K *et al* 2019 Cancer cell migration on elongate protrusions of fibroblasts in collagen matrix *Sci. Rep.* **9**
[77] Röhrig M, Thiel M, Worgull M and Hölscher H 2012 3D Direct laser writing of nano- and microstructured hierarchical gecko-mimicking surfaces *Small* **8** 3009–15
[78] Oran D *et al* 2018 3D nanofabrication by volumetric deposition and controlled shrinkage of patterned scaffolds *Science* **362** 1281–5
[79] Mih J D *et al* 2011 A multiwell platform for studying stiffness-dependent cell biology *PLoS One* **6** e19929
[80] Sun J-Y *et al* 2012 Highly stretchable and tough hydrogels *Nature* **489** 133–6
[81] Li J, Illeperuma W R K, Suo Z and Vlassak J J 2014 Hybrid hydrogels with extremely high stiffness and toughness *ACS Macro Lett.* **3** 520–3